Electronic Supplementary Material (ESI) for Soft Matter.

Electronic Supplemental Information

Claudio Maggi,[a,b†] Matteo Paoluzzi,[c] Andrea Crisanti,[b,d] Emanuela Zaccarelli,[d,b] and Nicoletta Gnan [d,b‡]

Center of mass shifting

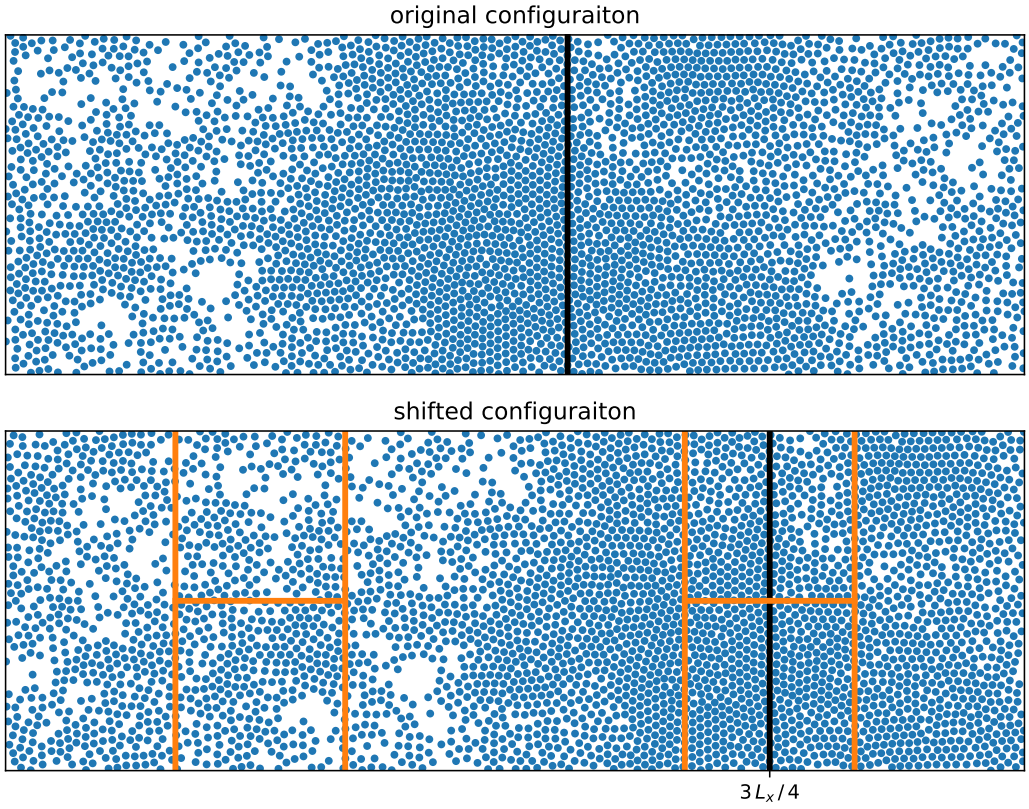

Fig. 1 (Top-panel) One original configuration for $N = 3750$, $\rho = 0.95$ and $\tau = 16.5$. The x-coordinate of the center of mass found is indicated by the black vertical line. (Bottom-panel) Shifter veriosn of configuration in top panel. Particles positions are shifted so that the x-coordinate of the center of mass coincides with $3L_x/4$. The analysis sub-boxes (orange lines) are centered onto $3L_x/4$ (dense phase) and onto $L_x/4$ (dilute phase).

We analyze the data following the same procedure of Ref.[1] and used also in Ref.[2]. For each configuration we first find the x-coordinate of the center of mass with periodic boundary conditions as shown in Fig. 1(top). We then shift particles coordinate so that the center of mass x-coordinate coincides with $3L_x/4$ (see Fig. 1(bottom)). Finally we perform the analysis on the sub-boxes (orange lines) that are centered onto $3L_x/4$ (dense phase) and onto $L_x/4$ (dilute phase) as shown in Fig. 1(bottom).

Length of the simulation runs

We show here that the length of the simulation runs is long enough to allow the full relaxation of the density correlation function $C(t) = \langle \Delta N_b(0) \Delta N_b(t) \rangle / \langle \Delta N_b{}^2 \rangle$, where $\Delta N_b = N_b - \langle N_b \rangle$ is the fluctuation of the number of particles in the sub-box. More specifically we analyze separately the relaxation in the dense and dilute phases considering the two sub-boxes on the left and two on the right as shown

[a] *NANOTEC-CNR, Institute of Nanotechnology, Soft and Living Matter Laboratory - Piazzale A. Moro 2, I-00185, Roma, Italy*
[b] *Dipartimento di Fisica, Università di Roma "Sapienza", I-00185, Roma, Italy*
[c] *Departamento de Fisica de la Matèria Condensada, Universitat de Barcelona, C. Martì Franquès 1, 08028 Barcelona, Spain*
[d] *CNR-ISC, Institute of Complex Systems, Roma, Italy*
[†] *E-mail: claudio.maggi@cnr.it*
[‡] *E-mail: nicoletta.gnan@cnr.it*

in Fig 1 of the main text. Figure 2(a) and (b) display $C(t)$ for the largest system investigate (i.e $N = 60 \times 10^3$) at different τ values both in the dense and dilute phase: in both cases $C(t)$ decay to zero at all τ.

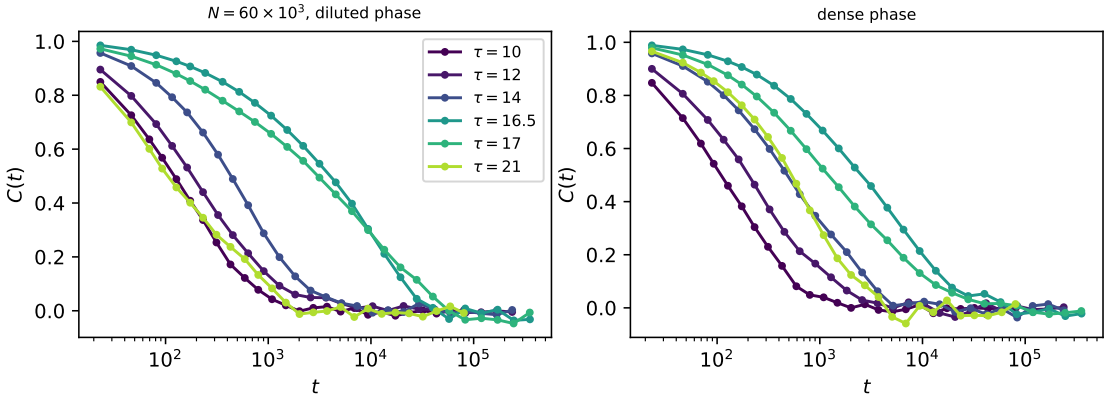

Fig. 2 Density auto-correlation function for the system with $N = 60 \times 10^3$ particles at $\rho = 0.95$ and different values of τ. Left panel: dilute phase. Right panel: dense phase.

Averages and error estimation

All quantities appearing in the main text (i.e. the Binder cumulant, the susceptibility, the order parameter and the kinetic temperature difference between the dense and dilute phase) are averaged over 16000 to 36000 configurations and over all sub-boxes. Individual configurations are taken at time intervals of duration ≈ 23 in reduced units, which is approximately equal the largest τ explored. Moreover for the values of τ close to τ_c these quantities of interest are averaged over multiple initial random configurations (up to 12 for the largest system sizes). To estimate the error on these quantities we proceed as follows: we first divide each run in time windows larger than the relaxation time of the density correlation function $C(t)$ (Fig. 2) we than compute the observable in each time-window and compute the standard error of the mean over all time windows. In Fig. 2 of the main text we report the error as twice the standard error of the mean. We have also checked that by computing the average of the Binder cumulant over these time windows (instead that on all configurations) we get almost identical results than those reported in Fig. 2 of the main text.

Estimate of the critical ρ and τ

We roughly estimate the critical density by performing a density scan, at fixed τ, in the proximity of the critical point for the smallest system investigated (i.e. $N = 3750$). According to Ref.[3] the cumulant should exhibit a maximum at $\rho = \rho_c$ when plotted as a function of ρ and at fixed $\tau = \tau_c$. Fig. 3(a) shows that the Binder parameter indeed displays a maximum if we fix $\tau = 16$. This value has been chosen based on preliminary simulations and it is close to the critical value $\tau_c = 16.36$ estimated in the following. Note also that the cumulant varies much less upon changing density in this small interval than upon changing τ on a large interval as in Fig. 2(a) of the main text. This is shown in the inset of Fig. 3(a) plotting the same data of the main panel in the y-range $(0.3;1)$, i.e. the range of the Binder cumulant as a function of τ. To extract ρ_c we have fitted the six closest points to the maximum in Fig. 3(a) with a 2nd order polynomial finding $\rho_c = 0.953(0.037)$ where the fit error is reported in brackets. We set the value $\rho_c = 0.95$ for all the sizes discussed in the main text neglecting the dependence of ρ_c on the size of the system.

The critical value τ, indicated by τ_c, has been determined by finding the crossing of the cumulants for two sizes $N = 15 \times 10^3$ and $N = 60 \times 10^3$. These have been chosen because $N = 60 \times 10^3$ is the largest size simulated and $N = 15 \times 10^3$ has a linear size which is two times smaller than the largest one. The procedure followed to find the intersection is illustrated in Fig. 3(b). We linearly interpolate the cumulant curves and find τ_c as the x-intersection of the two lines, while the critical cumulant value $\mathscr{B} = [\langle \Delta\rho^2 \rangle^2 / \langle \Delta\rho^4 \rangle]_{\tau=\tau_c}$ is found from the intersection on the y-axis. We obtain $\tau_c = 16.361(0.058)$ and $\mathscr{B} = 0.781(0.017)$. This $\mathscr{B}$ value is lower than the one found for the triangular lattice gas ($\mathscr{B} = 0.8321(0.0023)$, see section below) and for the square lattice gas ($\mathscr{B} \approx 0.83$ extracted from Ref.[1]). However it is close to $\mathscr{B} \approx 0.75$ which is the critical cumulant value of the active lattice model found in Ref.[2]. Note that previous studies on the Lennard-Jones fluid have also reported a lower value of the critical Binder parameter with respect to the Ising model[4].

To further check the size dependence of τ_c and $\mathscr{B}$, we have repeated this procedure also considering other system sizes, that are separated by a factor of 2 in linear size, i.e.: $(N = 3750, N = 15 \times 10^3)$ and $(N = 7500, N = 30 \times 10^3)$. The resulting $\tau_c(N)$ and $\mathscr{B}(N)$ are shown in Fig. 3(c) and (d) respectively where each value of $\tau_c(N)$ and $\mathscr{B}(N)$ is associated with the smallest size in the pair. In Fig. 3(c) and (d) we see that the values of both quantities at $N = 7500$ are closer to those of the largest system size (dashed lines) than to those corresponding to $N = 3750$. This suggests that, upon increasing the size, $\tau_c(N)$ and $\mathscr{B}(N)$ progressively converge to the infinite-system

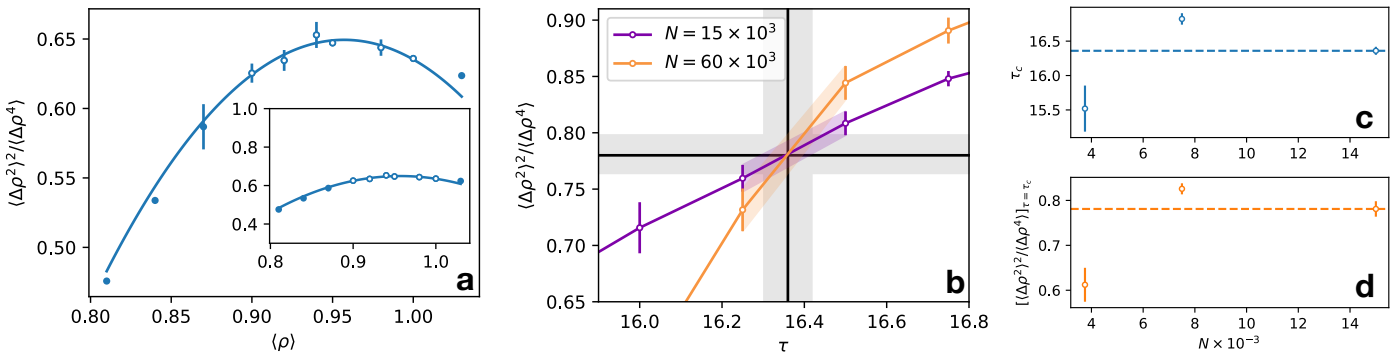

Fig. 3 (a) Fourth order cumulant as a function of density. Data points represent the Binder parameter varying the density at fixed $\tau = 16$ and $N = 3750$. The open symbols are the closest six points to the maximum used in the parabolic fit (full line) for determining ρ_c. The inset shows the same data of the main panel plotted on the same y-range of Fig. 2(a) of the main text. (b) Intersection of the cumulants (colored points) for $N = 60 \times 10^3$ and $N = 15 \times 10^3$ used for locating τ_c. The intersection point $\tau_c = 16.361(0.058)$ and $\mathscr{B} = 0.781(0.017)$ (black lines) is found by a piece-wise interpolation of the cumulant curves. The error on τ_c and $\mathscr{B}$ (gray areas) is obtained by propagating the y-error on the points nearby the intersection (colored areas). (c) and (d) (same x-axis) show the obtained values of τ_c and $\mathscr{B}$ (open symbols) as a function of the system size. The values of the reference point for the largest size is also reported as a dashed line.

critical values.

Direct estimates of the critical exponents

Here we show how we directly estimate the critical exponents. Following Ref.[1] we first focus on the dependence of the slope of the critical Binder cumulant on L whose scaling with size is controlled by the exponent ν:

$$\left[\frac{\partial}{\partial\tau}\left(\frac{\langle\Delta\rho^2\rangle^2}{\langle\Delta\rho^4\rangle}\right)\right]_{\tau=\tau_c} \sim L^{1/\nu} \tag{1}$$

To use Eq. (1) we evaluate the derivative of the cumulant by fitting the numerical data with a generalized logistic function of the form

$$y(\tau) = A_1 + \frac{A_2}{[A_3 + A_4\, e^{-(\tau-\tau_0)/w}]^{1/\theta}} \tag{2}$$

Where $A_1, A_2, A_3, A_4, w, \tau_0$ and θ are fitting parameters. As shown in Fig. 4(a) this function fits well the data especially around τ_c and allows us to estimate the derivative (1). This derivative is reported in Fig. 4(b) as a function of the system size and it is indeed well fitted by $\sim L^{1/\nu}$ with $\nu = 1$. In fact a direct fit with a power law gives $1/\nu = 0.968(0.096)$ (the fit error is indicated in brackets) and, by linear error propagation, $\nu = 1.03(0.10)$. Contrarily the best fit with the exponent $\nu = 1.5$ proposed in Ref.[1] deviates considerably from the data.

Next we consider the size dependence of the susceptibility χ at τ_c (i.e. $\chi_{\tau=\tau_c}$), that should scale as $\chi_{\tau=\tau_c} \sim L^{\gamma/\nu}$. To do this we simply linearly interpolate the χ at τ_c at all sizes and report the results in Fig. 4(c). This quantity is also well fitted by the Ising exponent $\gamma/\nu = 7/4 = 1.75$. A direct fit with a power law yields $\gamma/\nu = 1.787(0.090)$. Using ν found above and propagating also its error we get $\gamma = 1.84(0.20)$. Also in this case by fixing the values of $\gamma = 2.2$ and $\tau = 1.5$ (i.e. $\gamma/\nu \approx 1.47$) from Ref.[1] we obtain a worse fit of our data.

To directly estimate β we interpolate the points of the order parameter $(\rho_h - \rho_l)$ at τ_c for all sizes and we plot them as a function of L in Fig. 5(a). It is evident that these points are quite noisy and also that β/ν is small. However we are still able to obtain an estimate of β compatible with the Ising value ($\beta = 0.125$) when we fit these points with a power law $(\rho_h - \rho_l) \sim L^{-\beta/\nu}$. This yields $\beta/\nu = 0.110(0.053)$ (full line in Fig. 5(a)) and $\beta = 0.113(0.055)$ if the error on ν is propagated linearly. Note that this is close to the Ising value as shown by the orange line in Fig. 5(a) and appreciably smaller than the $\beta = 0.45$ of Ref.[1] shown by the green line Fig. 5(a).

To obtain a more accurate estimate of β we also implement a finer method which finds the exponent by minimizing the deviation between collapsed data. This type of technique has been applied in the past to extract the critical exponents of various spin models[5,6]. To practically apply this method we fix the values of τ_c and ν to the values determined above ($\tau_c = 16.36$ and $\nu = 1.03$). We then consider the following error function to be minimized:

$$\mathscr{E} = \sum_i \left[L_i^{\beta/\nu} m(\tilde{\tau}_i, L_i) - G(\tilde{\tau}_i)\right]^2 \tag{3}$$

where L_i and $\tilde{\tau}_i = L_i^{1/\nu}(\tau_i - \tau_c)$ are respectively the system size and the scaled control parameter of the i-th data-point, while $m(\tilde{\tau}_i, L_i) = [\rho_h - \rho_l]_{(\tilde{\tau}=\tilde{\tau}_i, L=L_i)}$ is the order parameter value at L_i and $\tilde{\tau}_i$ (the sum runs over all available data). The function G in Eq. (3) is the scaling

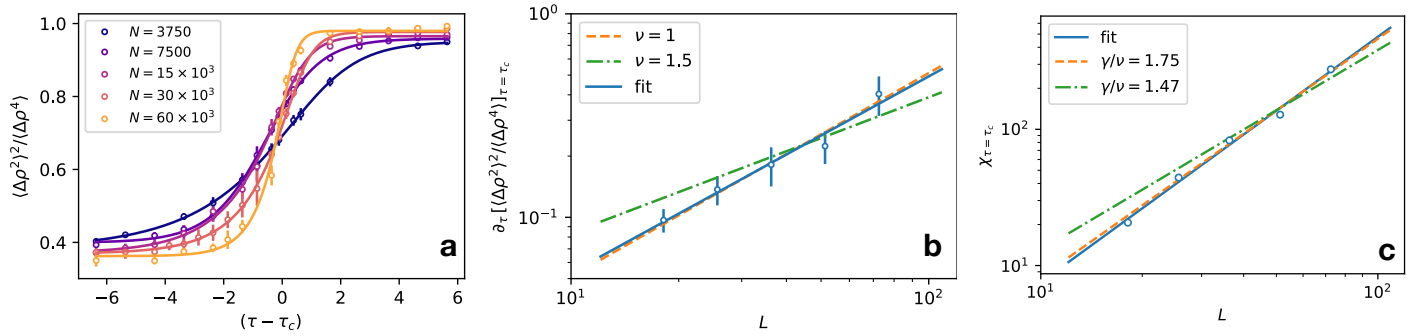

Fig. 4 (a) Fits of the Binder cumulant for estimating its derivative near τ_c. (b) Slope of the cumulants as a function of size. Solid line is the best fit of data points which gives $\nu = 1.03$. Orange dashed line is the best fit fixing $\nu = 1$ while green dashed-dotted line is the best fit with $\nu = 1.5$ from Ref.[1]. (c) susceptibility as a function of size. Solid line is the best fit of data points which gives $\gamma/\nu = 1.787$. Orange dashed line is the best fit fixing $\gamma/\nu = 1.75$ while the green dashed-dotted line is the fit with $\gamma/\nu = 1.47$ taken from Ref.[1].

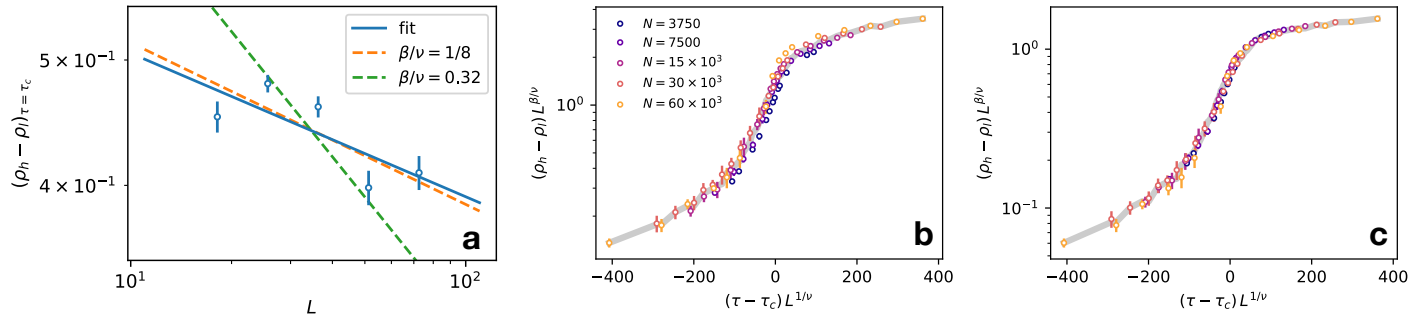

Fig. 5 (a) Order parameter as a function of size at $\tau = \tau_c$. Solid line is the best fit of data points which gives $\beta/\nu = 0.110(0.053)$ (i.e. $\beta = 0.113(0.055)$). Orange dashed line is the best fit fixing $\beta/\nu = 0.125$ while the green dashed-dotted line is the fit with $\beta/\nu = 0.32$ taken from Ref.[1]. (b) Collapsed order parameter data-points (colored dots) on the interpolating function (gray thick line) with exponent $\beta/\nu = 0.32$ from [1], the distance of the points from the interpolating function is large resulting in a large $\mathscr{E}$. (c) Same as (b) but with the fitted parameter $\beta/\nu = 0.130$ minimizing the $\mathscr{E}$ function.

function describing the critical behavior of m whose analytic form is unknown. To circumvent this problem we evaluate the function G by interpolating the values of $L^{\beta/\nu} m(\tilde{\tau}, L)$ with a smooth function. We compute G by averaging over windows of fixed size $\Delta\tilde{\tau}$ which we choose to be 10 times smaller than the overall $\tilde{\tau}$ range, i.e. $\Delta\tilde{\tau} = \max(|\tilde{\tau}_i|)/10$. In this way a smoothed G can be evaluated at each desired value $\tilde{\tau}_i$. An example of the resulting G is plotted in Fig. 5(b) where we use the parameter $\beta/\nu = 0.32$ of Ref.[1]. It is clear that, while the resulting G is smooth enough, the simulation data-points do not collapse well on the curve. The value of β/ν which minimizes the $\mathscr{E}$ function of Eq. (3) is $\beta/\nu = 0.130(0.018)$ that results in a good data collapse as shown in Fig. 5(c) and is again compatible with the Ising value $\beta/\nu = 0.125$. This gives $\beta = 0.133(0.022)$, by linear error propagation, which is also compatible with the Ising value.

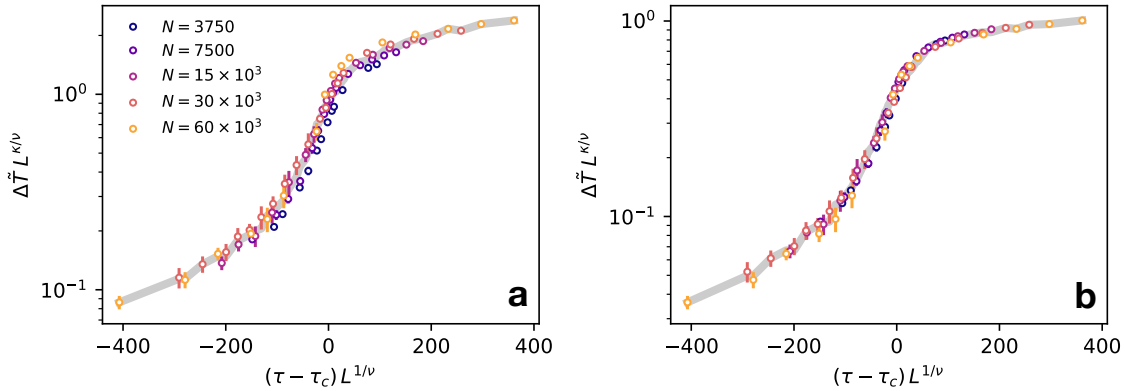

Fig. 6 Collapsed kinetic temperature difference $\Delta\tilde{T}$. (a) Colored dots represent the values of $\Delta\tilde{T}$ collapsed on the interpolating function (gray thick line) with exponent $\kappa/\nu = 0.32$. (c) Same as (b) but with the fitted parameter $\kappa/\nu = 0.118$ minimizing the $\mathscr{E}$ function.

Finally we estimate the exponent characterizing the critical behavior of the difference between the particle average squared speed of the dilute and dense phases, i.e. the quantity: $\Delta\tilde{T} = \frac{1}{2}(\langle|\dot{\mathbf{r}}|^2\rangle_l - \langle|\dot{\mathbf{r}}|^2\rangle_h)$. We use again the collapse optimization method introduced

above for estimating β (see Eq. (3)). In Fig. 6(a) we report the $\Delta\tilde{T}$ values if we use the exponent $\kappa/\nu = 0.32$. It is evident that, with this exponent, the data-points do not collapse well on the interpolating function (gray curve in Fig. 6(a)). Minimizing the $\mathscr{E}$-function we obtain $\kappa/\nu = 0.118(0.018)$ (i.e. $\kappa = 0.122(0.022)$) which gives a good data collapse as shown in Fig. 6(b).

Scaling behavior of the susceptibility and of the order parameter in the 2d equilibrium lattice gas

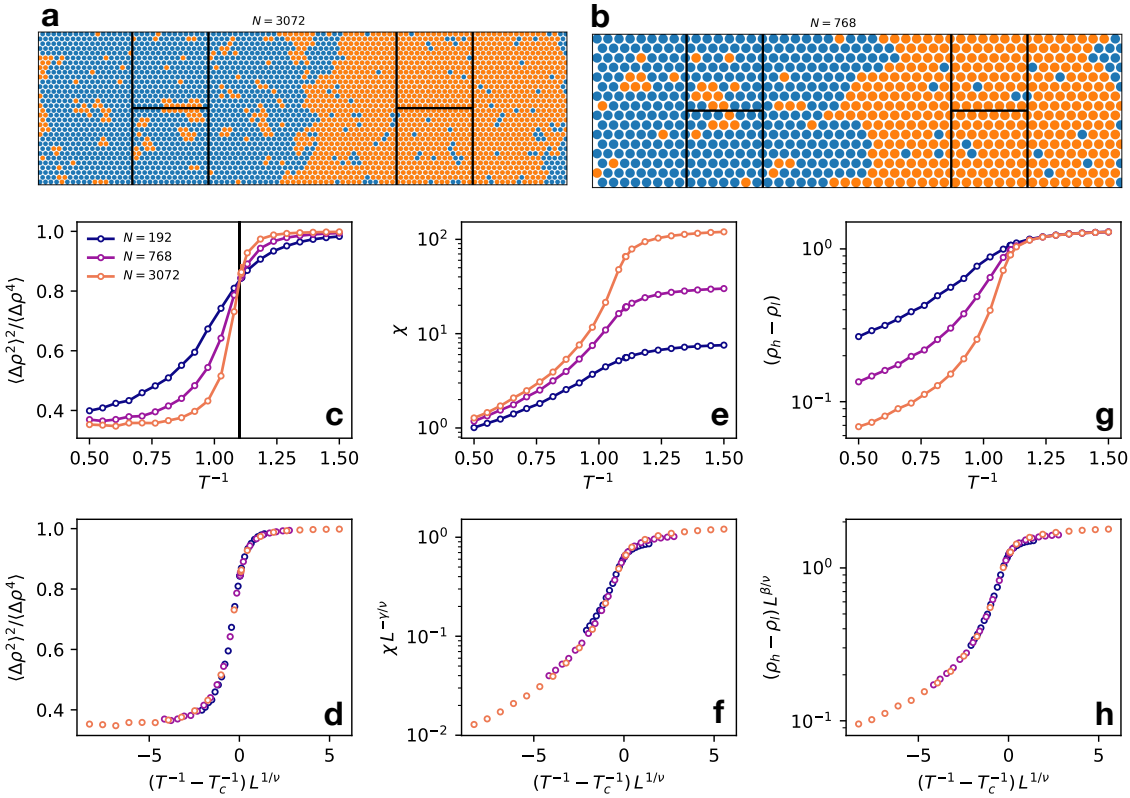

Fig. 7 (a) and (b) Near-critical configurations of an equilibrium lattice gas on the triangular lattice in a rectangular geometry for two different sizes (at $T^{-1} \approx 1.13$). Blue points represent empty sites while orange points represent occupied sites. The configuration is shifted so that the dense phase is centered on the right boxes (located at $x = 3L_x/4$, black lines) and the dilute phase is centered on the left sub-boxes (at $x = L_x/4$). (c) Binder cumulant for the lattice gas as a function of inverse temperature for different sizes (see legend), the vertical line corresponds to the exact $T_c^{-1} \approx 1.1..$ (d) Data collapse of the data in (c) with $\nu = 1$. (e) Susceptibility for the lattice gas as a function of inverse temperature for different sizes. (f) Data collapse of the data in (e) with $\nu = 1$ and $\gamma = 7/4$. (g) Order parameter as a function of the inverse temperature for the lattice gas for various sizes indicated in the legend (the order parameter is computed as the average density difference between the sub-boxes on the right and on the left). (h) Data collapse of the data in (h) using the exponents $\beta = 1/8$ and $\nu = 1$.

To check whether the susceptibility and the order parameter behave in the same qualitative way in the active system and in equilibrium we consider a lattice gas on a triangular lattice in a rectangular geometry (similar to the one employed for the active system). We simulate systems of three different sizes composed by $N = 192$, 768 and 3072 sites. These sites are enclosed in a rectangular box of size $(0, L_x) \times (0, L_y)$ with $L_x = aN_x$ and $L_y = a\sqrt{3}N_y/2$, where $a = 1$ is the lattice spacing. In all simulations we set $N_x = 3N_y$ and $N = N_x \times N_y$ is the total number of sites. Some near-critical configurations lattice gas simulated is shown in Fig. 7(a) and (b). By imposing periodic boundary conditions every site has 6 neighbours and the total lattice gas Hamiltonian ($H_{\rm lg}$) is given by

$$H_{\rm lg} = -J \sum_{\langle i,j \rangle} n_i n_j \,, \tag{4}$$

where J is the coupling constant set to 1 for convenience and n_i is the occupancy of the i-th site which assume the values 0 or 1. The simulations conserve the total occupancy (i.e. $\sum_i n_i = \text{const}$) by using a Kawasaki-type dynamics[7] in which a site can exchange its occupancy with any other site in the lattice in order to accelerate the approach to equilibrium. After an occupancy switch is proposed a standard Monte Carlo (MC) Metropolis rule is applied and the new configuration is accepted or rejected according to the energy change. All simulation results are obtained at fixed average occupancy $\sum_i n_i/N = 0.5$ (i.e. at the critical occupancy), starting from a random configuration (i.e. at infinite temperature). It is possible to show, via the transformation $n_i = (1 + \sigma_i)/2$, that the model (4) can

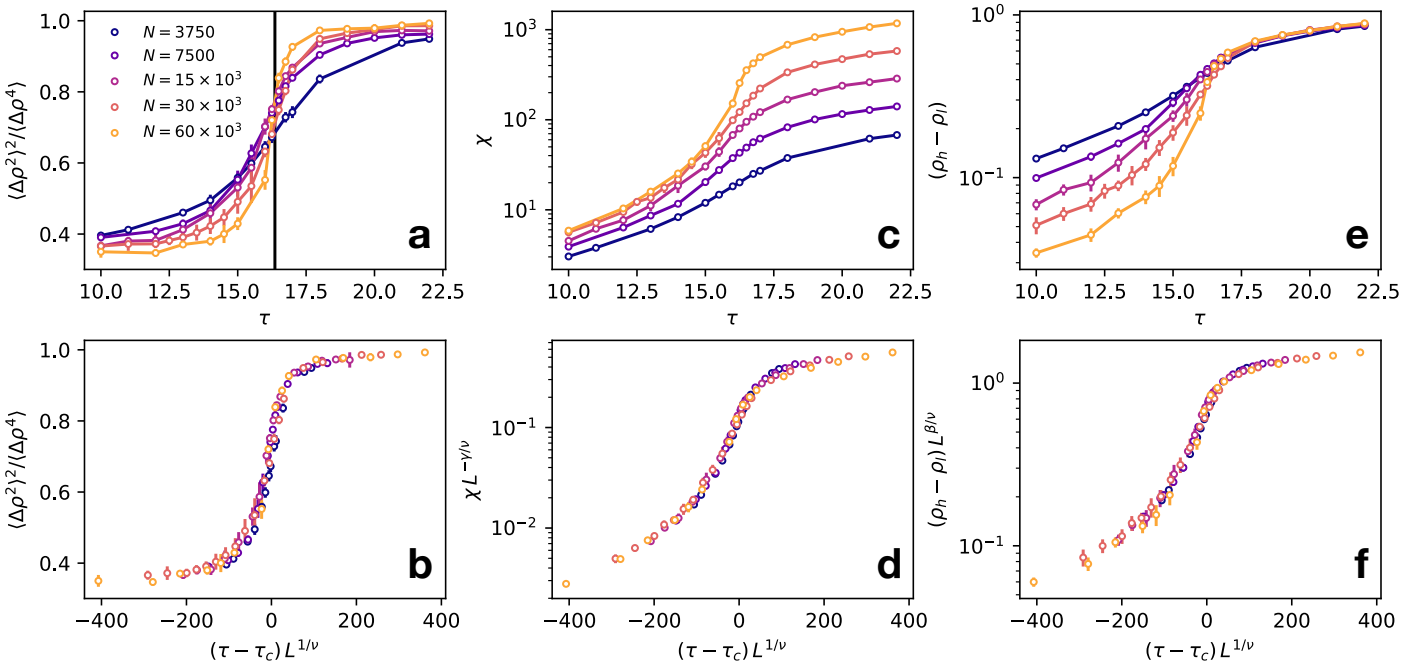

Fig. 8 Data collapse of the analyzed quantities with the exponents estimated directly $\nu = 1.03$, $\gamma = 1.84$ and $\beta = 0.133$ (including the smallest system with size $N = 3750$).

be mapped onto the Ising model with spin $\sigma_i = \pm 1$ on the triangular lattice having critical temperature $T_c = 4/\ln 3 \approx 3.641$ (for $J = 1$ and $k_B = 1$)[8]. As a consequence, the T_c of the lattice gas model turns out to be $T_c = 1/(\ln 3) \approx 0.91$, i.e. an inverse critical temperature $T_c^{-1} \approx 1.099$ while the critical average occupancy is $n_c = 0.5$.

The configurations of the lattice gas are analyzed as described in the main text for the active system. We start by shifting each configuration so that the its center of mass is positioned at $x = 3L_x/4$ as also shown in Fig. 7(a) and (b). Subsequently the quantities of interest are averaged over all four $L \times L$ sub-boxes, where $L = L_y/2$. The density ρ in one sub-box is computed as $\rho = \sum_i' n_i/L^2$, where the prime indicates the sum runs only on those sites within the sub-box. Using this method we further check the correctness of the critical temperature by showing the Binder parameter and its good scaling with $\nu = 1$ in Fig.s 7(c) and (d). By interpolating and averaging the values of the cumulants at the known value of T_c for all sizes we get $\mathscr{B} = 0.8321(0.0023)$ which is close to the value of $\mathscr{B}$ of the square lattice gas found in Ref.[1]. In the main text we have mentioned that the χ, computed by averaging over all sub-boxes, does not show the typical peaked shape but rather forms a s-shaped curve when plotted as a function of the control parameter. This is the case also for the equilibrium lattice gas as shown in Fig. 7(e). In Fig. 7(f) we also show that this χ scales well with $\nu = 1$ and $\gamma = 7/4$. In the main text we have also used the average difference of the density in the high-density phase ρ_h and of the low-density phase ρ_l as an order parameter. To check if this quantity behaves as expected at criticality also in the equilibrium case we compute ρ_h and ρ_l as the average density of the two sub-boxes on the right and on the left respectively. The resulting $(\rho_h - \rho_l)$ is shown in Fig. 7(b) as a function of T^{-1}. In Fig. 7(c) we show that we obtain a good data collapse by using the Ising exponents $\beta = 1/8$ and $\nu = 1$. These data are clearly compatible with those presented for the off-lattice active system discussed in the main text, thus reinforcing the robustness of the analysis bringing to the Ising universality class in the case of the active system.

System sizes, hexatic order and velocity correlation length

We discuss here the data collapse for the smallest system simulated, i.e. $N = 3750$ (not included in the main text), which is comparable with the sizes used in a previous investigation on the critical behaviour of an off-lattice active system[1]. For this size, in Fig. 8 (a)-(c), we report the Binder cumulant, the susceptibility and the order parameter. It is evident that a reasonable data collapse with the exponents calculated above is found also for $N = 3750$ (see Fig. 8(b),(d) and (f)). However the crossing point of the Binder cumulant for this size seems significantly lower in $\mathscr{B}$ and τ than the larger sizes (see also Fig. 3(c) and (d)). As mentioned in the main text we speculate that this could be due to the presence of another growing (but not diverging) correlation length. In the following we identify and compare two of them: the first related the hexatic order and the second associated to velocity correlations.

A very recent work[9] has shown that the dense phase formed by active particles undergoing MIPS is made of a mosaic of hexatic micro-domains whose size does not diverge. To compare the size of these regions with our smallest system size, near the critical point, we consider the state point $\tau = 16.5$, $\rho = 0.95$ for $N = 3750$. In Fig. 9(a) we show a high-resolution density map of one configuration of this system (near τ_c, already showing phase separation). This ρ-map is obtained by counting the number of particles in small squared

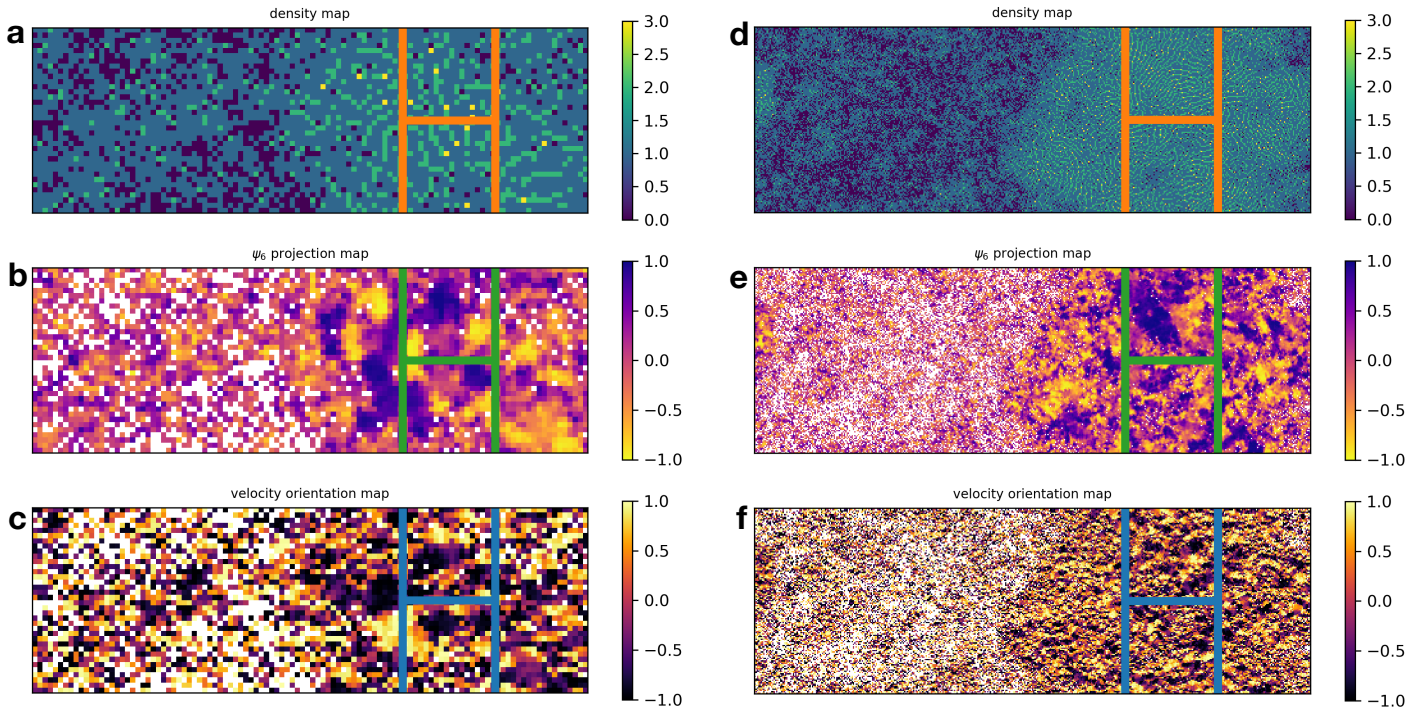

Fig. 9 (a), (b) and (c) represent, respectively the maps of the density field, the ψ_6 projection and the velocity direction projection for a typical configuration of sytem with $N = 3750$, $\tau = 16.5$ and $\rho = 0.95$. The map is calculated for a single configuration choosing bins of the order of the particles size. Different colors represent different values of the fields (see color-bars on the right). White pixels in (b) and (c) correspond to bins where no particles are found. The dense-phase sub-boxes (employed for the FSS) are drawn on (a), (b) and (c) to compare its size with the size of hexaitc andvelocity-oriented domains. (d), (e) and (f) are the same of (a),(b) and (c) respectively but for a configuration of a large system ($N = 60 \times 10^3$, $\tau = 16.5$ and $\rho = 0.95$).

bins of linear size $s = 1$. To characterize the hexatic order we calculate the parameter $\psi_{6j} = N_j^{-1} \sum_k e^{i\theta_{jk}}$ for each particle. Here θ_{jk} is orientation angle of the segment connecting the position of the j-th particle with its k-th (out of N_j) nearest neighbors found with a Voronoi tessellation. To visualize the regions with the same orientation we project ψ_{6j} onto the direction of the mean orientation $N^{-1} \sum_i \psi_{6i}$ where the sum runs over all particles in the system. In Fig. 9(b) we show the ψ_6-projection map obtained by averaging the ψ_6-projection of the particles found in each small bin (white pixels correspond to empty bins). In Fig. 9(b) it is evident that, in the dense phase, hexatic domains (i.e. regions with the same color) have an extent comparable to the size L of the FSS analysis boxes (we have $L \approx 18$ for $N = 3750$).

Recent works [10,11] have also shown that in active systems the colored noise induces an effective coupling between particles velocities. This effect gives rise to regions of densely packed particles with correlated speed and velocity orientation. We show here that, close to τ_c, these regions have a size similar to the one of the hexatic regions. To visualize the extent of these velocity correlations we show in Fig. 9(c) the orientation map of particle velocities. This map is obtained by averaging the projected particle velocity vector on the x-axis, i.e. $\cos(\vartheta_j)$ (where ϑ_j is the orientation angle of the j-th particle velocity). Fig. 9(c) shows that the "islands" of velocity-correlated particles have a size comparable with the size of hexatic regions. Note however that when we consider a larger system ($N = 60 \times 10^3$ and $L \approx 72$) at the same τ and ρ that is phase separating (Fig. 9(d)) the extension of these correlated hexatic and velocity regions does not scale up but remains approximately of the same size (see Fig. 9(e) and (f)). To quantify this more precisely we compute the correlation function of the hexatic order parameter $g_6(r) = \langle \psi^*_{6j} \psi_{6k} \rangle_{|\mathbf{r}_k - \mathbf{r}_j| = r} / \langle |\psi_{6j}|^2 \rangle$ and the correlation function of the velocity orientation vector $g_{\hat{\mathbf{v}}}(r) = \langle \hat{\mathbf{v}}_j \cdot \hat{\mathbf{v}}_k \rangle_{|\mathbf{r}_k - \mathbf{r}_j| = r}$. These functions are computed and reported in Fig. 10 considering only particles in the dense phase of the largest system. We find that both g_6 and $g_{\hat{\mathbf{v}}}$ decay to zero in an exponential-like fashion as shown in the double-log inset Fig. 10. We assume that both correlators are well described by a Ornstein-Zernike form in q-space (i.e. $g(q) \sim (\xi^{-2} + q^2)^{-1}$) and therefore we fit both data-sets with a function of the form $g(r) = A K_0(r/\xi) + B$ where K_0 is the modified Bessel function of the second kind ξ is the correlation length and A and B are amplitude and shift factors. The fit is quite good and reveals (in agreement with the qualitative map analysis discussed above) that the typical correlation lengths of the hexatic domains and velocity-oriented domains are, respectively, $\xi_6 = 9.9(1.2)$ and $\xi_{\hat{\mathbf{v}}} = 4.89(0.15)$.

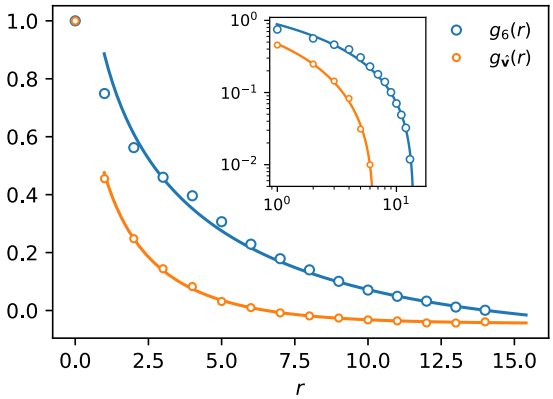

Fig. 10 Spatial correlation function of the hexatic order parameter ψ_6 (blue points) and of the velocity orientation vector (orange points, see legend) for particles in the dense phase for the system with ($N = 60 \times 10^3$, $\tau = 16.5$ and $\rho = 0.95$). The full lines are fits with the $K_0(r/\xi)$ Bessel function. The inset is the same of the main panel but on a double-log scale.

References

1 J. T. Siebert, F. Dittrich, F. Schmid, K. Binder, T. Speck and P. Virnau, Physical Review E, 2018, **98**, 030601.

2 B. Partridge and C. F. Lee, Phys. Rev. Lett., 2019, **123**, 068002.

3 M. Rovere, D. W. Heermann and K. Binder, Journal of Physics: Condensed Matter, 1990, **2**, 7009.

4 M. Rovere, P. Nielaba and K. Binder, Zeitschrift für Physik B Condensed Matter, 1993, **90**, 215–228.

5 S. M. Bhattacharjee and F. Seno, Journal of Physics A: Mathematical and General, 2001, **34**, 6375.

6 J. Houdayer and A. K. Hartmann, Physical Review B, 2004, **70**, 014418.

7 A. Bovier and F. den Hollander, in Metastability, Springer, 2015, pp. 425–457.

8 L. Zhi-Huan, L. Mushtaq, L. Yan and L. Jian-Rong, Chinese Physics B, 2009, **18**, 2696.

9 C. B. Caporusso, P. Digregorio, D. Levis, L. F. Cugliandolo and G. Gonnella, arXiv preprint arXiv:2005.06893, 2020.

10 L. Caprini, U. M. B. Marconi and A. Puglisi, Physical Review Letters, 2020, **124**, 078001.

11 L. Caprini, U. M. B. Marconi, C. Maggi, M. Paoluzzi and A. Puglisi, Physical Review Research, 2020, **2**, 023321.